Structural Chemistry
https://doi.org/10.1007/s11224-018-1149-6

ORIGINAL RESEARCH

Synthesis, characterization, pharmacological, molecular modeling and antimicrobial activity evaluation of novel isomer quinoline derivatives

S. Murugavel[1] · S. Sundramoorthy[2] · R. Subashini[3] · P. Pavan[4]

Received: 15 March 2018 / Accepted: 21 June 2018

Abstract
The structural and spectroscopic characteristics of the synthesized structurally novel compound 4-chloro-6-methylquinoline-2(1H)-one (4C6MQ) and its isomer 4-chloro-8-methylquinoline-2(1H)-one (4C8MQ) have been examined by means of experimental and computational quantum chemical methods like density functional theory (DFT). The crystal structure of the 4C6MQ compound has been brought to light by single-crystal x-ray diffraction (SCXRD) method which consists of two independent molecules (A and B) in the asymmetric unit with similar conformations. Both the isomer compounds are characterized spectroscopically by FTIR, FT-Raman, UV-Vis, and NMR spectrum and compared with DFT results. The geometries of the isomer compounds have been optimized by using DFT/B3LYP method with the 6-311G++(d,p) basis sets. From the optimized geometry of the compounds, geometric parameters (bond lengths, bond angles, and torsion angles); vibrational analysis; chemical shifts; and electronic absorption of the isomer compounds have been computed and compared with the experimental result. The detailed assignments of vibrational wave numbers have been prepared based on potential energy distribution (PED) which was carried out in the VEDA4 program. In addition, natural bonding orbital analysis, frontier molecular orbital, and molecular electrostatic potential have been explained theoretically. The in silico (absorption, distribution, metabolism, excretion and toxicity) studies were analyzed to identify the potential drug likeliness of the isomer compounds. The implications of the inhibitory activity of isomer compounds against DNA gyrase and lanosterol 14 α-demethylase enzyme by molecular docking are discussed. Further, the isomer compounds were screened for their antibacterial and antifungal activities.

Keywords 4-Chloromethyl quinoline (4CMQ) isomer · SCXRD · Spectral · DFT · Pharmacological and molecular docking · Antimicrobial activity

Electronic supplementary material The online version of this article (https://doi.org/10.1007/s11224-018-1149-6) contains supplementary material, which is available to authorized users.

✉ S. Murugavel
smurugavel27@gmail.com

[1] Department of Physics, Thanthai Periyar Government Institute of Technology, Vellore, Tamil Nadu 632002, India

[2] Department of Physics, Saveetha Engineering College, Thandalam, Chennai, Tamil Nadu 602105, India

[3] Department of Chemistry, Arignar Anna Govt. Arts College for women, Walajapet, Vellore, Tamil Nadu 632513, India

[4] Organic Chemistry Division, School of Advanced Sciences, VIT University, Vellore, Tamil Nadu 632014, India

Introduction

Quinoline consists of a benzene ring connected to a pyridine ring which is at its proximity. Most of the quinoline derivatives that are extracted from their natural sources or those which are prepared synthetically are more significant in medicinal chemistry and biomedical use [1]. Normally, quinoline is widely utilized as antimalarial [2], antibacterial [3], antituberculosis [4], antifungals [5], and anticancer agents [6].

Quinoline compounds are broadly used as "parental" compounds to synthesize molecules with medical benefits, especially for antimalarial [7–9], antimicrobial [10–13], and anticancer activities [14]. This wide range of biological and biochemical functions has been further facilitated by the synthetic

Published online: 02 July 2018

versatility of quinoline, which permits generating a large number of structurally varied byproducts.

Different functional groups, such as, halogens, nitro, and methoxy have an effective importance in medicinal chemistry. The addition of halogen, oxygen, and other substitution to quinoline ring has shown great alteration in molecular structure, charge distribution, optical properties, and biological activities [15, 16]. Specifically, the halogen-like chloro, as in antifungal azoles offers an effective antifungal activity [17]. 2-Quinolone or quinolin-2(1H)-one and their derivatives exhibit a wide spectrum of valuable biological activities, particularly antimicrobial effect [18, 19], antioxidant agents [20], and anticancer and antitumor activities [21, 22]. Literature review has been motivated to synthesis the chloro quinolone derivative.

To the best of our knowledge, the isomer compounds are synthesized and structurally characterized by single-crystal x-ray diffraction (SCXRD), NMR, FTIR, FT-Raman, and UV-Vis for the first time. Hence, the isomer compounds are structurally novel.

The present paper discusses about the synthesis of the 4-chloro-6-methylquinoline-2(1H)-one (4C6MQ) and its isomer 4-chloro-8-methylquinoline-2(1H)-one (4C8MQ) [23] and also explores the structural properties of the same using spectral (NMR, FTIR, FT-Raman, UV-Vis) studies and compares it with the density functional theory (DFT) calculations. The crystal structure of 4C6MQ has been investigated by SCXRD method and compared with the DFT studies. The properties of the structural geometry, molecular electrostatic potential (MEP), natural bond orbital (NBO) analysis, and chemical reactivity descriptors have been investigated for 4-chloromethyl quinoline (4CMQ) isomer. We also have made comparisons between experimental and computational calculations.

Since literature survey reveals that the chloro quinolone derivative exhibits antimicrobial activity, docking studies has been carried out against the bacterial protein DNA gyrase enzyme and fungal protein lanosterol 14 α-demethylase enzymes.

DNA gyrase, which is situated in the bacterial cell cytoplasm, is an essential enzyme for bacterial pathogen [24]. The DNA gyrase inhibition disturbs the production of DNA and finally onsets the death of the pathogen. This makes them as an effective target for antibacterial drugs. Hence, the isomer compounds were docked into DNA gyrase enzyme.

The lanosterol 14 α-demethylase (CYP51) enzyme is the most imperative catalyze for ergosterol biosynthesis process. The key role of antifungal compound is affecting the CYP51 function and to stop the production of ergosterol in fungi, which is essential for fungal cell membrane activity [25]. The disturbance of ergosterol production subsequently decreased the cellular protection causing outflow of cellular substances and ultimately results in cell death. The lanosterol 14α-demethylase enzyme has been known for a long time as an effective target for antifungal drugs. Hence, the isomer compounds were docked with lanosterol 14α-demethylase enzyme.

A molecular docking outcome for 4CMQ isomer recommends that the compounds might exhibit inhibitory activity against microbial strain. The results of molecular docking inspired us to perform anti-bacterial and antifungal activities.

Experimental and computational methods

Synthesis

The synthetic route leading to the target isomer compounds is depicted in Scheme 1. When equimolar mixture of methyl substituted anilines (**1**), (0.001 mol) and malonic acid (**2**), (0.001 mol) were refluxed with 30 ml of phosphorous oxy chloride on a heating mantle maintained at a temperature of 80–100 °C for 5 h, 2,4-dichloromethyl quinolines (**3**) were synthesized [26]. On completion of the reaction (monitored by TLC), the reaction mixtures were cooled and poured slowly onto the crushed ice with continuous stirring. The solid thus separated was filtered, dried, and washed thoroughly with water. Column purification (95:5 hexane/EtOAc) of the crude solid gave 2,4-dichloromethyl quinoline (**3**), in a good yield. The isomer compounds, (**4**) have been synthesized by refluxing (**3**) with 20 ml of 4 N HCl for 30 min. The solid thus separated was filtered and washed thoroughly with

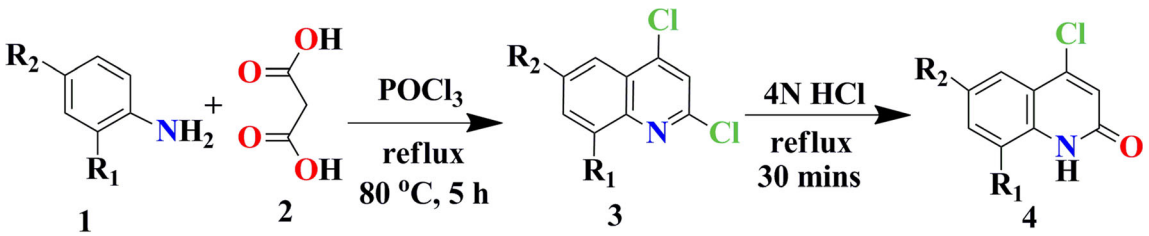

4C6MQ: R_1= H; R_2= CH_3
4C8MQ: R_1=CH_3; R_2= H

Scheme 1 Synthesis of 4-chloromethyl quinoline-2(1H)-one (4CMQ) isomer

distilled water and then dried to obtain the compounds 4C6MQ and 4C8MQ. The compound 4C6MQ was dissolved in ethanol and single crystals were developed by slow evaporation at room temperature.

4-chloro-6-methylquinoline-2(1H)-one, 4a White solid, 82.6% yield, and mp 236–238 °C. IR (KBr) cm^{-1}: 856, 1667, 2823, and 3450. Proton NMR (DMSO-d_6, 300 MHz) δ: 2.42 (3H, s, CH_3); 6.06 (1H, s, CH); 7.23 (2H, m, CH); 7.6 (1H, s, CH); and 11.8 (1H, s, NH). Carbon-13 NMR (DMSO-d_6, 75 MHz) δ: 22.1, 115.6, 117.3, 121.2, 2 × 122.8, 131.8, 138.4, 141.3, and 160.3. Mol. formula: $C_{10}H_8ClNO$.

4-chloro-8-methylquinoline-2(1H)-one, 4b White solid, 74.4% yield, and mp 232–234 °C. IR (KBr) cm^{-1}: 856, 1647, 2906, and 3430. Proton NMR ($CDCl_3$, 400 MHz) δ: 2.42 (3H, s, CH_3); 6.06 (1H, s, CH); 7.23 (2H, m, CH); 7.6 (1H, s, CH); and 11.7 (1H, s, NH). C-13 NMR ($CDCl_3$, 100 MHz) δ: 55.7, 124.2, 125.6, 126.4, 129.3, 130.5, 142.7, 144.1, 147.1, and 159.0. Mol. formula: $C_{10}H_8ClNO$.

Experimental

Spectral measurements

Infrared absorption spectral data in this work was collected using a PerkinElmer Spectrum one FTIR spectrophotometer. FTIR measurements were recorded between the frequency 4000 and 450 cm^{-1}. Bruker RFS27 FT-Raman spectrophotometer with an external 300-mW diode laser operating at 785 nm as source was used throughout this work. The proton and carbon-13 NMR spectra have been carried out using Bruker AVANCE-III spectrometer with TMS as internal standard and $CDCl_3$ as solvent. The UV-absorption spectra were examined in the range 500–190 nm using a PerkinElmer lambda 35 UV-Vis spectrophotometer (spectral bandwidth is 1 nm).

Crystallography

A suitable 4C6MQ fine crystal with dimensions 7.51 mm × 8.57 mm × 14.55 mm was mounted on a goniometer using cyanoacrylate adhesive and data collection was performed on a Bruker AXS Kappa APEX II-CCD diffractometer [27] utilizing the ω scan technique with graphite-monochromatic MoK_α radiation (wave length λ = 0.71073 Å) at room temperature (293 K). The systematic absence and intensity symmetries confirm the triclinic $P\bar{1}$ space group. A total of 17,254 reflections (3742 unique) were obtained within the θ range 2.51° to 26.75°. Empirical absorption correction (μ = 0.385 mm^{-1}) was attained by the integration method via SADABS [28] program.

SHELXS-97 [29] implemented in WINGX [30] was utilized in the solvation of the molecular structure by direct methods. The positional and anisotropic temperature parameters were refined by the full-matrix least squares technique based on F^2 utilizing SHELXL-97 for all atoms except for hydrogen. All hydrogen atoms were located geometrically and were constrained to be dependent on their parent atom with the bond lengths at 0.86, 0.93, and 0.96 Å for NH, CH, and CH_3 atoms, respectively. Due to interference from the beam stop, the poor reflections (− 1 0 1), (2–4 4) and (0 0 1) were eliminated from the final cycles of refinement.

The general purpose crystallographic software such as PLATON [31], ORTEP [30], and MERCURY [32] were used for the structure analysis and demonstration of the results. Complete details of the crystal data, restraints and the parameters of the refinement process for 4C6MQ are given in Table 1.

Antimicrobial activity

The 4CMQ isomer compounds were screened for their antimicrobial activity and compared with available standard drugs like ciprofloxacin for bacteria and fluconazole for fungi. The bacterial activity for the isomer compounds was screened against *Escherichia coli*, *Staphylococcus aureus*, *Pseudomonas aeruginosa* with nutrient niger, *Monascus purpureus*, and *Penicillium citrinum* with nutrient sabouraud dextrose agar medium by applying DMSO as solvent. The antimicrobial activities were assayed by Kirbybauer disk diffusion method [33] under the guidelines of CLSI M38-A [34]. Each 4CMQ isomer compound was dissolved separately in DMSO solvent at 25, 50 and 75 μg/ml concentration and screened against selected microbial pathogens. The test compounds having antimicrobial behavior inhibit bacterial/fungal growth in the media nearby the discs and thereby produced clear distinct areas that are defined as the zone of inhibition in millimeter.

Computational details

DFT

All the quantum chemical computations of the isomer compounds have been carried out using the GAUSSIAN 03 program package [35]. The geometries of the compounds were optimized at the hybrid density functional B3LYP with the 6-311++G(d,p) basis set [36, 37].

Frequency analyses also were performed using the same basis set to generate calculated infrared and Raman spectra. Furthermore, not even a single imaginary wave number is available in the predicted vibrational spectrum, entailing that the optimized geometries are situated at the local minimum energy on the potential surface. We realized that the

Table 1 Crystallographic data and refinement parameter for 4C6MQ

Empirical formula	$C_{10}H_8ClNO$
Formula weight	193.62
Temperature	293 K
Wavelength	0.71073 Å
Crystal system	Triclinic
Space group	$P\bar{1}$
Unit cell dimensions	
A	7.5173 (3) Å
B	8.5757 (4) Å
C	14.5572 (6) Å
α	96.355 (2)°
β	96.193 (9)°
γ	106.632 (2)°
Volume	884.01 (7) $Å^3$
Z	4
Density (calculated)	1.455 g^{-3}
Absorption coefficient	0.385 mm^{-1}
F (000)	400
Crystal size	0.23 × 0.21 × 0.16 mm^{-3}
Theta range for data collection	2.51 to 26.75°
Index ranges	$-9 \le h \le 7, -10 \le k \le 10, -18 \le l \le 18$
Reflections collected	17,254
Independent reflections	3742 [$R_{int} = 0.0264$]
Completeness to theta = 26.75°	99.3%
Absorption correction	Semi-empirical from equivalents
Max. and min. transmission	0.915 and 0.940
Refinement method	Full-matrix least squares on F^2
Data/restraints/parameters	3742:0:237
Goodness-of-fit on F^2	1.000
Final *R* indices [*I* > 2 sigma (*I*)]	$R1 = 0.0387$, $wR2 = 0.1051$
R indices (all data)	$R1 = 0.0488$, $wR2 = 0.1147$
Largest diff. peak and hole	0.563 and −0.550e $Å^{-3}$

computation wave numbers are typically higher than the experimental result. These discrepancies arise due to the avoidance of anharmonicity effects, the incomplete association of electron correlation, and the use of basis set in the computational treatment. These discrepancies are rectified by scaling with a factor of 0.958 for the high-energy-level vibrational bands (above 1700 cm^{-1}) and a factor of 0.983 for the low-energy-level vibrational bands (below 1700 cm^{-1}) [38, 39]. Based on the potential energy distribution (PED), the computational normal mode wave number of the isomer compounds were interpreted by utilizing VEDA 4 program [40].

Gauge-independent atomic orbital (GIAO) proton (^1H) and carbon-13 (^{13}C) NMR chemical shifts of isomer compounds have been computed by the B3LYP/6-311++G (d,p) method. TD-DFT method with 6-311++G (d,p) basis has been used to compute the electronic absorption spectra for 4CMQ isomer compounds in the chloroform solvent phase. Further, uppermost filled orbital-lowermost empty orbital (HOMO-LUMO) and molecular electrostatic potential diagrams were obtained using the same level theory.

Pharmacological investigation

The drug likeness analysis on the basis of Lipinski rule of five and molecular parameter score of isomer compounds were computed by Molinspiration online server [41]. The Lipinski's "rule of five" [42] has four physiochemical parameters such that molecular weight, miLogP, number of H-bond donor and number of H-bond acceptors. Here, five represent limits of these parameters which are multiples of five. The organic compounds are considered orally active if the molecular weight (MW) is lower than 500 g per mole; miLogP value does not exceed five; number of H-bond acceptor value is below ten, and number of H-bond donor value does not exceed five [43]. Lipinski rule of five is essentially used to decide, whether the compound with a specific biological activity is an orally dynamic drug or not. The pharmacological properties like absorption, distribution, metabolism, excretion and toxicity (ADMET) for isomer compounds were carried out using Pre-ADMET online server [44].

Molecular docking

Molecular docking studies are computational methods for exploration of probable interaction between a substrate and a given receptor, enzyme, or other binding site. The docking studies of each isomer compound were performed using AutoDock 4.2 software [45] which was a suite of automated docking tools (ADT). The target protein DNA gyrase (PDB ID:3G75) and CYP51 (PDB ID:1EA1) retrieved from the protein data bank (www.rcsb.org/pdb). Prior to docking, the co-crystallized ligand, water molecules, and co-factors were removed from the target protein. The ADT graphical user interface helps to add polar hydrogen which are bonded with electronegative nitrogen and oxygen atoms and detection of Kollman charges within active sites of amino acids. The DFT/B3LYP/6-311++G(d,p) level optimized ligand structure was used for docking. By choosing a flexible and rigid molecule to generate grid map dimensions 60 Å × 60 Å × 60 Å along *x*-, *y*- and *z*-axis allocated to epicenter of the grid map *X*, *Y*, and *Z* coordinates of 8.25, −4.37, and 16.14 and −18.23, −7.97, and 65.96 for 3G75 and 1EA1 enzymes, respectively, and the molecular stimulation parameters of resultant compounds were computed by Lamarckian genetic algorithm [46]. The target protein with 4CMQ isomer compounds were docked individually and then ten optimum conformations were evaluated. The conformational protein structure is modeled and visualized using Discovery Studio Visualizer [47].

Results and discussion

Crystal structure

Crystals of the 4C6MQ belongs to the triclinic space group $P\bar{1}$ with two independent molecules (A and B) per asymmetric unit, which is shown in Fig. 1a. The unit cell constants of 4C6MQ are $a = 7.5173$ (3) Å, $b = 8.5757$ (4) Å, $c = 14.5572$ (6) Å, $\alpha = 96.355(2)°$, $\beta = 96.193$ (9)°, $\gamma = 106.632$ (2)°, $V = 884.01$ (7) Å^3, and $Z = 4$ (at 293 K). The supplementary information in the CIF form is available (refer supplementary materials) from Cambridge Crystallographic Database Centre, No. CCDC 928281.

The quinoline ring system [N1/C1–C9] of both molecules A and B are approximately planar [maximum deviation = − 0.014 (2) Å for atom N1A of molecule A and − 0.038 (2) Å for atom C7B of molecule B]. The Cl1A/O1A atom of molecule A and Cl1B/O1B atom of molecule B are deviated by − 0.034 (1)/0.004 (1) Å and − 0.052 (1)/0.090 (1) Å, respectively, from the attached quinoline ring system. In both molecules, the sum of bond angles around N1 [360.0°] specifies that the atom N1 is in sp^2 hybridization. A structural overlay of the two independent molecules A and B [RMS deviation for fitting all atoms = 0.050 Å] which shows a similar conformation and is depicted in Fig. 2. The geometrical parameters of molecules A and B are comparable with the reported values of similar quinoline derivatives [43, 48].

The hydrogen bond geometry for 4C6MQ is listed in Table 2. In both A and B, the molecular structure is stabilized by C2A–H2A … Cl1A and C2B–H2B … ClIB intra-molecular hydrogen bonds, each forming S(5) ring motifs. In the crystal, molecules A and B are inter connected by inversion dimers through intermolecular N1A–H1A … O1B^{i} and N1B–H1B … O1A^{i} [$i = -x, -y, -z$] hydrogen bonds, each generates an $R_2^2(8)$ ring motif. These dimers are further joined by intermolecular C–H … π interaction between a methyl atom H10A and pyridine ring (N1B/C1B/C6B/C7B–C9B) of an immediate molecule as an acceptor with a C10B–H10A … Cg3^{ii} [ii = $1 - x, -y, 1 - z$] separation of 2.85 Å and π–π interactions with Cg1 … Cg1^{iii}, Cg1 … Cg2^{iii}, Cg2 … Cg1^{iii}, Cg2 … Cg2^{iv}, Cg3 … Cg3^{v}, Cg3 … Cg4^{v}, and Cg4 … Cg3^{v} separation of 3.790 (1), 3.608 (1), 3.608 (1), 3.708 (1), 3.870 (1), 3.631 (1), and 3.631 (1) Å, respectively, [Cg1, Cg2, Cg3, and Cg4 are the centroids of the pyridine ring of molecule A, C1A–C6A ring, pyridine ring of molecule B and C1B–C6B ring, respectively, and symmetry codes: iii = $-x, 1 - y, -z$; iv = $1 - x, 1 - y, -z$, and $v = -x, -y, 1 - z$] making a three-dimensional supramolecular network as displayed in Fig. 3.

Optimized geometry

4CMQ isomers were initially simulated by DFT methods to scrutinize the molecular structures, along with the vibrational spectra. Their calculated geometrical structures and dimer of 4C8MQ were completely optimized using B3LYP/6-311++G(d,p) basis set as shown in Figs. 1b and 4. An interaction of CH3, Cl, and O with quinoline ring plays a significant part for defining the structural and

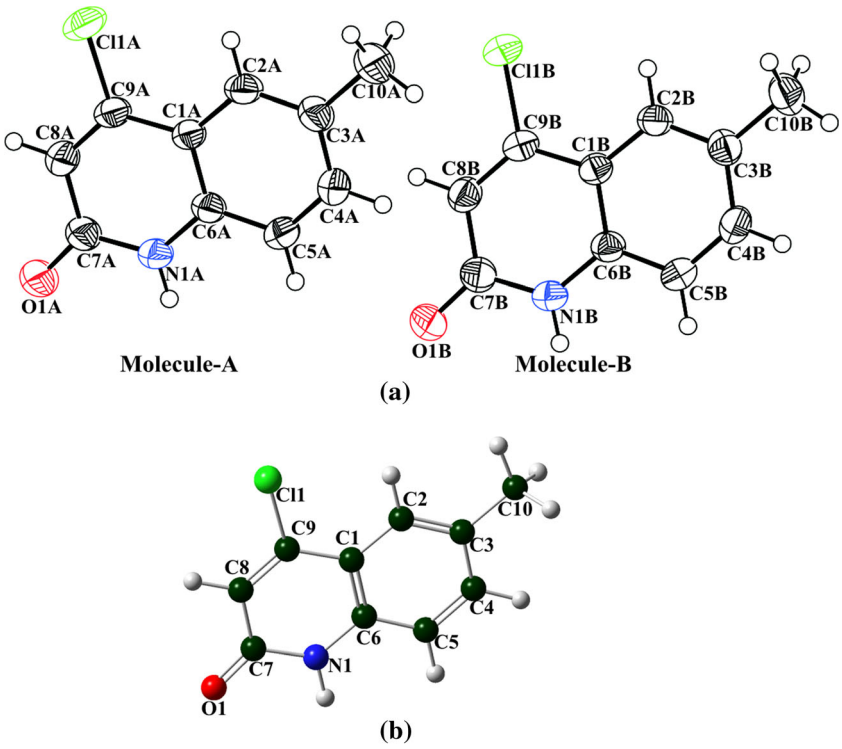

Fig. 1 View of 4C6MQ showing two crystallographically independent molecules A and B with the atom-numbering scheme (**a**). Displacement ellipsoids are drawn at the 50% probability level. The optimized geometric structure of 4C6MQ (**b**)

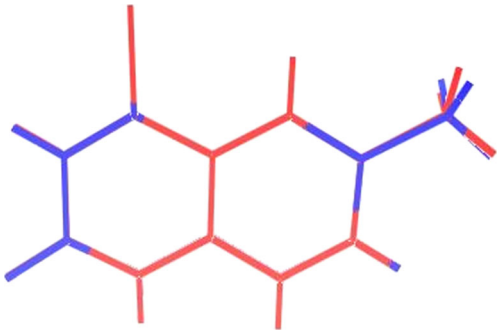

Fig. 2 The structural overlay of independent molecule A (red) and B (blue) of the 4C6MQ compound

vibrational properties of isomer compounds. These isomer structures have two carbon-nitrogen, seven carbon-hydrogen, one nitrogen-hydrogen, one carbon-oxygen, and nine carbon-carbon bond lengths. Binil et al. reported carbon-linked oxygen double-bond length as 1.2145 Å (DFT) and 1.23 Å (XRD) [49]. In this case, C=O bond length for both isomer compounds exactly coincides with reported value [43] (refer Table 3). The bond length between carbon and chlorine atom agrees quite well with Y. Sert et al's. reported result [50]. From Table 3, the bond angle C1–C9–C8 is expanded and the bond angles C1–C9–Cl1 and C8–C9–Cl1 are shrunken from perfect hexagonal angle (120°) due to the substitution of electronegative chlorine atom. The bond angles O1–C7–C8 and O1–C7–N1 are expanded and the bond angle N1–C7–C8 is shrunken from 120° due to the attachment of oxygen atom at C7 position. From this discussion, the substituted chlorine and oxygen atoms in the isomer compound leads to certain distortion in the bond lengths and bond angles of the pyridine ring. The steric interactions raise the small distortion among the experimental and computed result of the dihedral angles [51].

The minimum energy of the 4C8MQ monomer and dimer structures was evaluated by the DFT/B3LYP/6-311++G(d,p) computation as − 5,123,355.3509 and − 2,561,644.1678 kJ mol^{-1}, respectively. The dimer formation energy ($\Delta E = E_{dimer} - 2 \times E_{monomer}$) is equal to 16.0063 kcal mol^{-1}, which is equal to energy of two hydrogen bonds [52]. These predict that two N–H ... O hydrogen bonds are present in this dimer as shown in Fig. 4. The N–H … O hydrogen bond distance for 4C8MQ dimer is 1.831 Å and intermolecular hydrogen bond for 4C8MQ compound dimer structure is nearly linear (the N–H ... O angle is around 171.69°). Both isomer structures are different in the sense that the methyl group is attached to the C3 and C5 atom in 4C6MQ and 4C8MQ compound, respectively.

Table 2 Hydrogen bonding geometry for 4C6MQ (Å, °)

D–H … A	D–H (Å)	H–A (Å)	D–A (Å)	D–H … (Å)
C2A–H2A … Cl1A	0.93	2.68	3.070 (2)	106
C2B–H2B … Cl1B	0.93	2.69	3.077 (2)	106
N1A–H1A … O1B^{i}	0.86	1.98	2.829 (2)	171
N1B–H1B … O1A^{i}	0.86	1.95	2.813 (2)	176
C10B–H10A … Cg3^{ii}	0.96	2.85	3.646 (2)	141

Symmetry code: $i = -x, -y, -z$; ii = $1-x, -y, 1-z$

Cg3 is the centroid of the pyridine ring of molecule B

Vibrational spectra

Each isomer nonlinear compound has 21 atoms and 57 normal modes of vibration. These 57 vibration modes are classified by 20 stretching, 19 bending, and 18 torsion modes. The potential energy distribution (PED) for each normal mode among the symmetry coordinates of the molecules was computed. A wide-ranging assignment of the fundamentals was proposed based on the calculated PED values, infrared absorption intensities and Raman scattering activities. The experimental and theoretical infrared and Raman spectra of isomer compounds 4C6MQ and 4C8MQ are displayed in Figs. 5 and 6, respectively. The observed and scaled computed wave numbers along with other data are listed in Tables S1 and S2 (supplementary materials).

Ring vibration

Each isomer compounds have seven C–H stretching modes linked with ring and methyl group. The wave numbers resulting from the ring C–H stretching of isomer compounds fell in the spectral range 3000 −3100 cm^{-1}, which coincide with reported wave numbers [53, 54]. The aromatic C–H stretching vibration mode does not affect by the location and properties of the substitution in this region. In the present analysis, the isomer compounds show C−H absorption modes in the wave number region 3015−3098 cm^{-1} for FTIR and FT-Raman spectrum. The DFT/B3LYP/6-311++G(d, p) wave numbers for ring C–H stretching modes are best agreements with experimental data.

The wave number region 1625–1430 cm^{-1} has been assigned to ring carbon-carbon stretching vibration mode. Particularly, Varsanyi et al. quoted five bands (frequency range 1625–1590, 1590–1575, 1540–1470, 1460–1430, and 1380–1280 cm^{-1}) with variable intensity for ring vibration in the fingerprint region [55]. In this case, the C–C and C=C stretching vibration mode wave number are exactly coincided with theoretical and also reported value [43]. The ring vibration for FTIR and FT-Raman spectrum

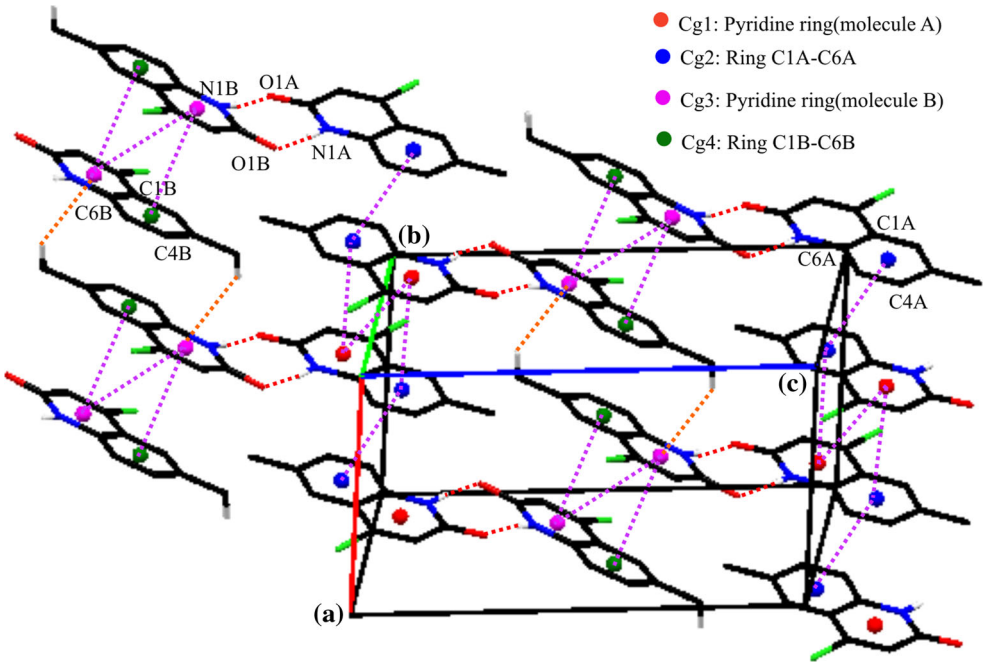

Fig. 3 View of a three-dimensional supra molecular network of 4C6MQ compound. The N–H ... O, π–π, and C–H … π interactions are shown as red, pink, and orange dotted lines, respectively

of isomer compounds were observed in the range 1496–1622 cm^{-1} which is in harmony with computational results (1440–1636 cm^{-1}).

N–H vibration

Obviously, heterocyclic compounds exhibits N–H stretching vibrations in the range 3500–3200 cm^{-1}[56]. In this investigation, N–H absorption spectrum appears at 3450 and 3430 cm^{-1} for isomer compounds 4C6MQ and 4C8MQ, respectively. This wave number is exactly coinciding with computational result of the both compounds. One hundred percent potential energy distribution value proves that this mode is pure. XRD data reveals that presence of hydrogen (N–H … O) bond in 4C6MQ and conforms that N–H stretching vibration was relocated to higher energy state which is caused by the protonation [43].

C–Cl vibration

The vibrations belong to C–Cl bonds which are formed between the ring and the chlorine atom. Chlorine-attached compounds absorb strongly in the region 760–505 cm^{-1} due to the C–Cl stretching vibration [57]. In the present case, the band absorbed at 856 cm^{-1} in FTIR spectrum due to C–Cl stretching vibration of both compounds. In FT-Raman, C–Cl bond gets absorbed at 874 and 843 cm^{-1} for the isomer compound 4C6MQ and 4C8MQ, respectively. Two impacts may be responsible for the change of

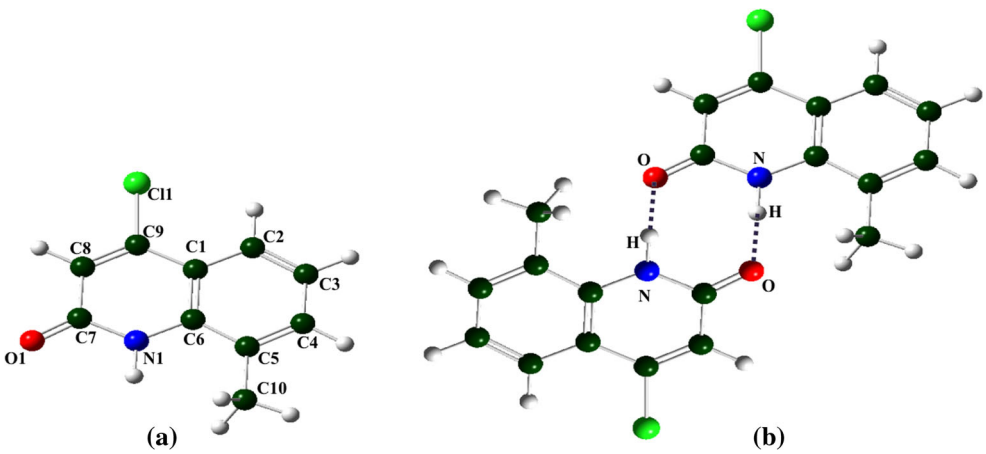

Fig. 4 The optimized geometry of 4C8MQ compound (**a**) with atoms numbering and its hydrogen-bonded dimer (**b**)

Table 3 Selected structural parameters for 4CMQ isomer

Parameters	4C6MQ		DFT	4C8MQ
	XRD			DFT
	Molecule A	Molecule B		
Bond lengths (Å)				
C3–C10	1.505 (2)	1.502 (2)	1.509	–
C6–N1	1.380 (2)	1.381 (2)	1.380	1.381
C7–O1	1.241 (2)	1.239 (2)	1.223	1.222
C7–N1	1.352 (2)	1.358 (2)	1.393	1.394
C9–CL1	1.727 (2)	1.728 (2)	1.757	1.757
C5-C10	–	–	–	1.508
Bond angles(°)				
C2–C3–C10	120.68 (17)	120.59 (17)	121.51	–
C4–C3–C10	121.22 (17)	121.14 (16)	120.47	–
N1–C6–C5	120.20 (15)	120.17 (15)	120.97	120.28
N1–C6–C1	119.90 (15)	119.96 (15)	119.54	118.89
O1–C7–N1	121.15 (16)	120.97 (17)	120.06	120.87
O1–C7–C8	122.98 (16)	123.26 (16)	124.85	124.95
N1–C7–C8	115.86 (15)	115.76 (15)	114.09	114.19
C8–C9–Cl1	119.28 (14)	119.35 (13)	118.59	118.45
C1–C9–Cl1	118.02 (13)	118.01 (12)	118.62	118.58
C7–N1–C6	124.80 (15)	124.70 (15)	125.91	126.29
C4–C5–C10	–	–	–	121.33
C6–C5–C10	–	–	–	120.72
Torsion angles(°)				
C1–C2–C3–C10	179.39 (18)	− 177.65 (16)	180	–
C4–C5–C6–N1	− 179.59 (17)	− 177.29 (16)	180	− 180
C2–C1–C6–N1	179.47 (16)	178.34 (15)	− 180	180
C9–C1–C6–N1	− 0.4 (2)	− 0.4 (2)	0	0
O1–C7–C8–C9	179.44 (19)	179.23 (17)	180	180
N1–C7–C8–C9	− 0.2 (3)	− 1.1 (3)	0	0
C7–C8–C9–Cl1	− 178.34 (15)	179.40 (13)	− 180	− 180
C6–C1–C9–Cl1	178.65 (14)	− 178.68 (12)	− 180	180
C2–C1–C9–Cl1	− 1.2 (3)	2.7 (2)	0	0
O1–C7–N1–C6	179.48 (17)	− 177.74 (16)	− 180	− 180
C8–C7–N1–C6	− 0.9 (3)	2.6 (3)	0	0
C5–C6–N1–C7	− 178.49 (18)	176.74 (17)	180	180
C1–C6–N1–C7	1.2 (3)	− 1.9 (3)	0	0
C3–C4–C5–C10	–	–	–	180
C10–C5–C6–N1	–	–	–	0
C1–C6–C5–C10	–	–	–	180

higher absorption frequency of C–Cl in isomer compounds. The first one is affected by vibrational coupling with other groups and another one is an inductive effect of C–Cl bond [43]. The computed wave number (862–851 cm^{-1}) of C–Cl stretching mode by B3LYP/6-311++G(d,p) agrees well with the experimental value.

C=O vibration

The stretching vibrations of carbonyl (C=O) typically appears in the frequency range 1700–1600 cm^{-1} [53]. In this investigation, FT-Raman band and FTIR band observed between the range 1647–1667 cm^{-1} for isomer compounds could be assigned to C=O stretching vibration. DFT computational wave number (at 1666 cm^{-1}) is in a noble agreement with the experimental result of the isomer compounds and related literature studies [58].

C–N vibration

In fingerprint region, identifying the carbon-nitrogen stretching vibration is a difficult job because this vibration mode seems to be superimposed with several internal vibrations. According to previous reports [59], carbon-nitrogen absorption band appears at 1382–1266 cm^{-1} due to C–N stretching vibration. In this study, the carbon-nitrogen stretching vibration is observed at 1254/1265 cm^{-1} (4C6MQ) in FT-Raman/FTIR and 1271/1274 cm^{-1} (4C8MQ) in FT-IR/FT-Raman spectrum. The PED of these modes are 22 and 17% for 4C6MQ and 4C8MQ, respectively. The low PED percentages prove that C–N mode is coupled with other vibration modes.

Methyl group vibration

For the assignments of methyl group frequencies, basically nine fundamentals can be associated to each CH_3 group, namely, symmetric stretch, asymmetric stretch, scissoring, and rocking which belongs to in-plane vibrations. In addition to wagging and twisting modes of CH_3 group, it would be expected to be depolarized for out-of-plane vibrations [55]. In our case, both 4C6MQ and 4C8MQ isomer compounds have one methyl group at the sixth and eighth position substitution in the quinoline ring, respectively. The bands in the region 2928–2985 cm^{-1} were assigned to asymmetric stretching mode of methyl group in isomer compounds. The symmetric stretching mode of methyl group has been identified in the region 2823–2906 cm^{-1}. The observed symmetry and asymmetry stretching mode wave numbers agreed with the computational result. The symmetric and asymmetric deformation mode wave numbers are gathered in the previous reported region (ref. Tables S1 and S2) [60].

The linear regression diagram of the experimental and computed wave numbers of isomer compounds in FTIR and FT-Raman is shown in Fig. S1 (supplementary materials). The regression depicts coherence between the experimental and computational wave numbers.

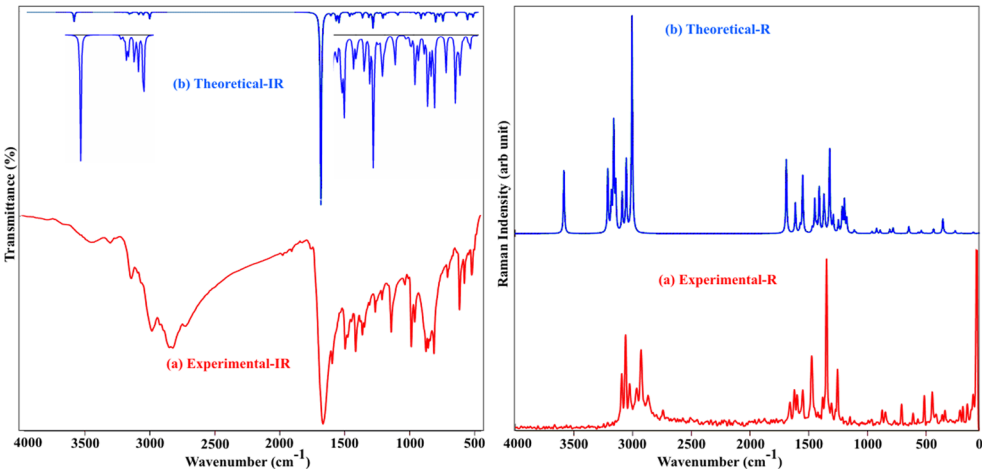

Fig. 5 Comparison of the experimental and theoretical IR and Raman spectra of 4C6MQ

NMR spectra

A nuclear magnetic resonance spectrum is playing a decisive role in identification of structural isomer molecules. In order to confirm the presence of predicted functional groups, the NMR spectra were analyzed in terms of their chemical shifts and splitting and integrations. The carbon-13 chemical shift is obtained as $\delta = \sigma_{ref} - \sigma$, where σ_{ref} is the shielding constant of carbon-13 in tetramethylsilane and σ is the same parameter in the molecule of interest [61]. The shielding constant of C-13 and proton NMR is 184.79 and 31.99 ppm, respectively.

Normally, the aromatic carbons chemical shifts are appeared in the range 90–160 ppm [62]. In our case, the chemical shifts of aromatic carbons found in the vicinity of 115–160(Exp)/120–165(DFT) ppm and 120–160(Exp)/125–165(DFT) ppm for 4C6MQ and 4C8MQ isomer compounds, respectively. In carbon-13 NMR, the fairly heavy atom oxygen and chlorine bound carbon atoms C7 and C9 as shows more deshielded (down field) than the others due to relativistic effects [63] as observed in Table 4. The isomer compound 4C6MQ/4C8MQ displays strong deshielded at C3/C5 atom owing to the attachment of methyl group. The methyl group carbon (C10) bonded with three hydrogen atoms has more shielding (up field) compared to other ring carbon atoms.

The proton NMR shows extremely deshielding and shielding effect on nitrogen-attached proton and three methyl protons, respectively, which have been proved from the chemical shift results (Table 4). The linear regression diagram of the computed and experimental chemical shifts of carbon-13 and proton nuclei have been shown in the Fig. S2 (supplementary materials). The regression depicts coherence between the experimental and computational chemical shifts.

NBO analysis

NBO analysis is one of the most information-rich and succinct tools for studying of hydrogen bonding and electron density delocalization from filled Lewis-type NBO to virtual non-Lewis-type NBO. The strength of interaction between Lewis and non-Lewis NBO is calculated based

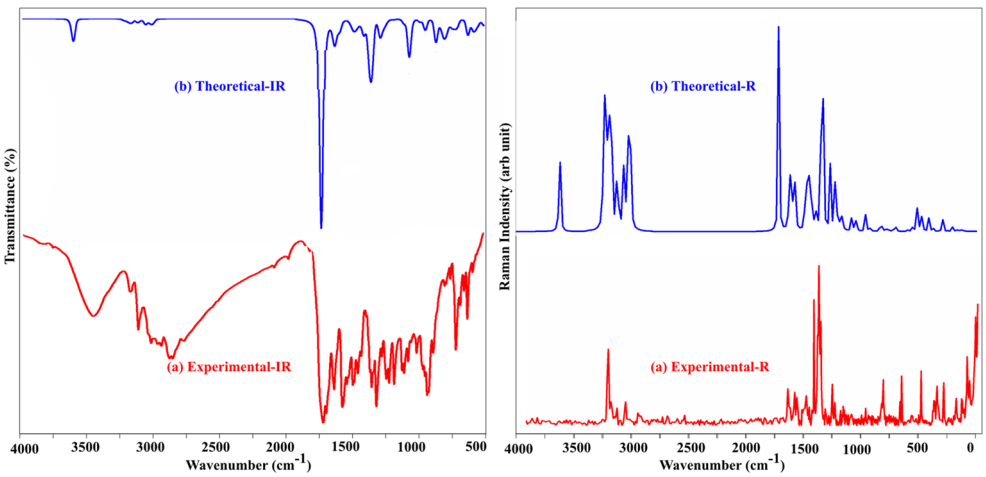

Fig. 6 Comparison of the experimental and theoretical IR and Raman spectra of 4C8MQ

Table 4 Comparison of B3LYP/6-311++G (d,p) calculated and experimental values of carbon-13 and proton chemical shift (ppm) relative to the TMS for 4CMQ isomer

Atom	4C6MQ		4C8MQ		Position
	Exp. value	DFT value	Exp. value	DFT value	
C1	117.3	124.95	122.6	125.16	(1C, Ar C)
C2	131.8	131.77	130.5	130.98	(1C, Ar C–H)
C3	138.4	144.86	–	–	(1C, Ar C–CH3)
	–	–	126.4	128.62	(1C, Ar C–H)
C4	122.8	141.03	142.7	140.32	(1C, Ar CH)
C5	115.6	121.51	–	–	(1C, Ar C–H)
	–	–	144.1	144.21	(1C, Ar C–CH3)
C6	122.8	141.26	129.3	130.64	(1C, Ar C)
C7	160.3	165.95	159.0	165.55	(1C, Ar C=O)
C8	121.2	127.35	124.2	127.34	(1C, Ar C–H)
C9	141.3	162.39	147.1	163.60	(1C, Ar C–Cl)
C10	22.1	23.27	55.7	18.63	(1C, C–H_3)
H1	11.8	8.41	11.72	8.24	(s, 1H, N–H)
H2	7.23	7.96	7.63	8.20	(d, 1H, Ar CH)
H3	–	–	7.8	7.60	(d, 1H, Ar CH)
H4	7.6	7.89	7.23	7.85	(t, 1H, Ar CH)
H5	7.23	7.43	–	–	(d, 1H, Ar CH)
H8	6.60	6.90	6.79	7.05	(s, 1H, Ar CH)
H10	2.42	2.61	2.41	2.48	(s, 3H, CH3)

on second-order perturbation theory. The stabilization energy related with delocalization of interacting filled (i) and virtual orbitals (j) is calculated using the relation [64],

$$E^{(2)} = q_i \frac{(F_{i,j})^2}{\varepsilon_j - \varepsilon_i}$$

where q_i is the filled orbital occupancy, ε_i and ε_j are (orbital energies) diagonal elements, and $F_{i,\ j}$ is the off-diagonal NBO Fock matrix element. If the stabilization energy is higher, then the strong interaction takes place between donors and acceptor orbitals [65]. In our compound 4C6MQ, π(C4–C5) → π*(C1–C6) has 21.14 kJ/mol, π(C2–C3) → π*(C4–C5) has 21.00 kJ/mol, and π(C8–C9) → π*(O1–C7) has 18.92 kJ/mol and hence they provide greater stabilization to structure. In 4C8MQ, π(C4–C5) → π*(C1–C6) has 21.58 kJ/mol, π(C2–C3) → π*(C4–C5) has 20.51 kJ/mol, and π(C8–C9) → π*(O1–C7) has 19.16 kJ/mol and hence they provide intense stabilization to structure. From Tables S3 and S4, chlorine, nitrogen, and oxygen had loan pair (LP) and the stabilization energy of LP(N) and LP(O) is 52.68:52.8 kJ mol^{-1} and 27.11:26.98 kJ mol^{-1} for 4C6MQ/4C8MQ, respectively. Owing to the higher stabilization energy value, these atoms are easily interacting with target protein active site which leads to strong binding energy between compound and target protein also, confirm the presence of N–H … O inter molecular hydrogen bond. The larger inter charge transmission occurs around the methyl group attached position in ring evident from the stabilization energy of π*(C4–C5) → π*(C2–C3) is 199.15 kJ/mol and π*(C6–C1) → π*(C4–C5) is 198.21 kJ/mol in 4C6MQ and 4C8MQ compounds, respectively. This enormous stabilization value represents larger delocalization of the NBO orbital. From the NBO analysis (ref. supplementary materials in Tables S3 and S4), it can be exposed that there is some vital charge transfer arising inside the isomer compounds, which is a symptom for the occurrence of bioactivity in molecule.

FMO and MEP

The computational molecular orbital shows that the first 50 molecular orbitals are occupied and the remaining (51 to 346)

Table 5 Calculated energy values of 4CMQ isomer by the B3LYP/6-311++G(d,p) approach

Parameters	4C6MQ	4C8MQ
Chemical hardness (η)	2.1580	2.2073
Chemical potential (μ)	−4.2990	−4.3407
Electro negativity (χ)	4.2990	4.3407
Softness (s)	0.2317	0.2265
Electrophilicity index (ω)	4.2821	4.2680

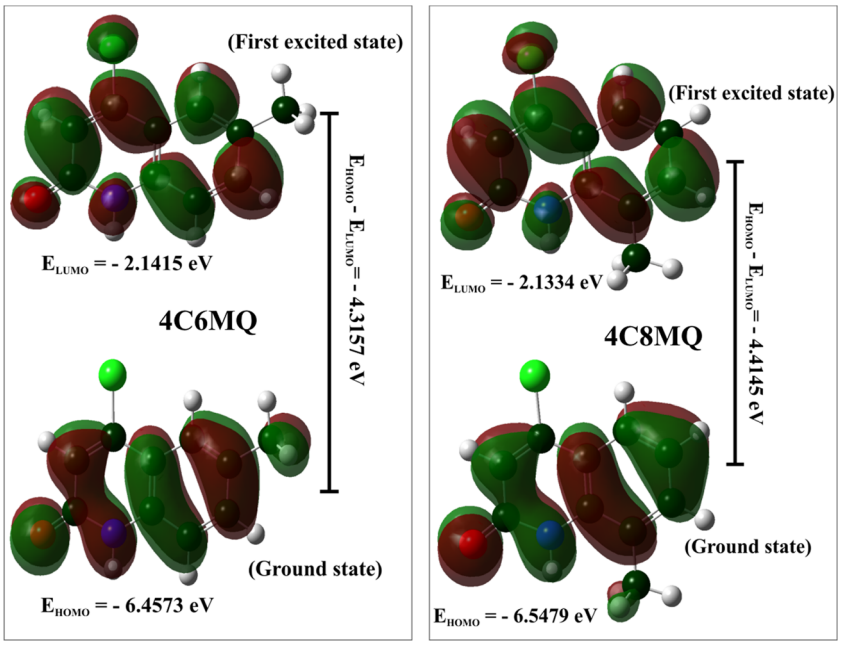

Fig. 7 The molecular orbital and energies for the HOMO and LUMO of 4CMQ isomer

molecular orbitals are empty for both isomer compounds. The energy value of uppermost filled orbital (HOMO), lowermost empty orbital (LUMO), and molecular orbital gap are found as − 6.4573, − 2.1415, and − 4.3157 and − 6.5479, − 2.1334, and − 4.4145 for 4C6MQ and 4C8MQ (Table 5), respectively, as shown in Fig. 7. Electron affinity and ionization potential of the compound are associated with E_{HOMO} and E_{LUMO}, respectively; that is, electron affinity $(I) = -E_{HOMO}$ and ionization potential $(A) = -E_{LUMO}$. Having the value of electron affinity and ionization potential, one could get the chemical hardness $\left(\eta = \frac{I-A}{2}\right)$ and electronegativity $\left(\chi = \frac{I+A}{2}\right)$ [61]. The chemical hardness values represent softness, stability, and inter molecular charge transfer (chemical reactivity) of the compound. In the present case, the low value of HOMO-LUMO energy gap in isomer compounds predicts intermolecular charge transfer occurs within the molecules which lead to biological dynamic behavior [66].

The MEP gives the complete details to identify the sites of nucleophilic and electrophilic attacks and charge distribution in molecular space based on different colors as per their polarity. The red and blue colors represent electrophilic and nucleophilic reactivity region as shown in Fig. 8. The color code of the current diagram is in the range from − 0.059 a.u (red) to 0.059 a.u (blue) for both the isomer compounds. The most nucleophilic region around N1–H1 atom which MEP value $V(r) = 0.049/0.042$ a.u. The oxygen atom (O1) has a high value of molecular electrostatic potential $V(r) = -0.059/-0.056$ a.u for 4C6MQ/4C8MQ compound which is in the maximum negative region. Thus, the result of MEP proves the presence of intermolecular N1−H1 … O1 hydrogen bond. The occurrence of nucleophilic and electrophilic rich region around nitrogen and oxygen atom, respectively, in isomer compounds indicates the significance of bioactivity for our synthesized compounds.

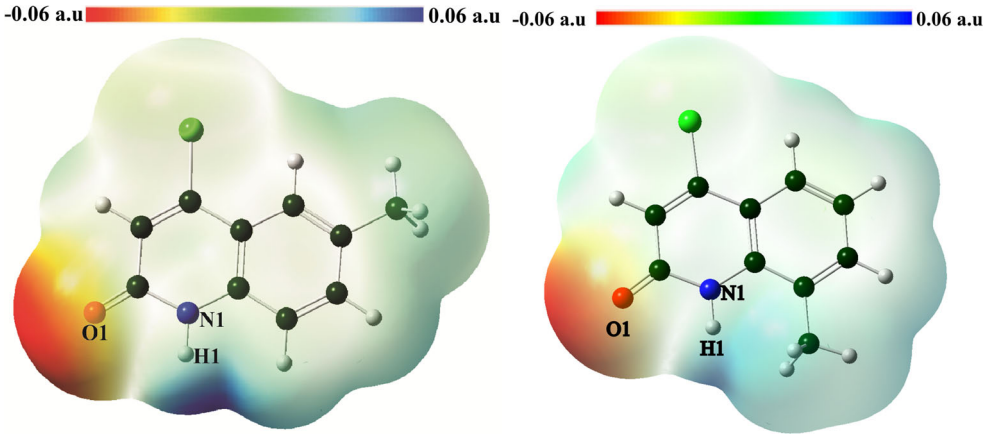

Fig. 8 Molecular electrostatic potential surface for 4CMQ isomer

Table 6 Theoretical and experimental electronic transitions, oscillator strength, and major contributions for 4CMQ isomer compound

Name	B3LYP/6-311++G(d,p)			Exp.	Assignments	Major contributions
	λ (nm)	*f*	*E* (eV)	λ (nm)		
4C6MQ	326	0.141	3.799	339	$n \rightarrow \pi^*$	$H \rightarrow L$ (85%)
	274	0.133	4.527	275	$\pi \rightarrow \pi^*$	$H-1 \rightarrow L$ (76%)
4C8MQ	321	0.130	3.868	345	$n \rightarrow \pi^*$	$H \rightarrow L$ (86%)
	279	0.166	4.441	233	$\pi \rightarrow \pi^*$	$H-1 \rightarrow L$ (78%)

H HOMO, *L* LUMO

Electronic absorption spectra

The electronic absorption spectra were induced in molecule by the electron jump from non-bonding or bonding molecular orbital to anti-bonding molecular orbital. Most possible transition types in organic materials are $\pi \rightarrow \pi^*$, $n \rightarrow \pi^*$ and π^*(donor) $\rightarrow \pi^*$(acceptor) [67]. In our case, electronic absorption UV spectra of the isomer compounds were computed using the time-dependent-DFT method with B3LYP/6-311++G(d,p) level-optimized structures in the chloroform solvent phase. The computed and experimental absorption spectra results have been listed in Table 6. From Table 6, computed value of absorption wave length was slightly deviated from the experimental results and both isomer compounds show homo → lumo transition has major contribution (85% for 4C6MQ and 86% for 4C8MQ) in absorption spectra. The strong $n \rightarrow \pi^*$ ($H \rightarrow L$) transition has major contribution in isomer compounds, which is proven from the highest delocalization value in NBO analysis. The computed and experimental absorption spectra of isomer compounds were shown in Fig. 9.

Pharmacological investigation results

The isomer compounds and standard drugs (ciprofloxacin and fluconazole) are uploaded in the Molinspiration online tool to evaluate the drug-likeness of the isomer compounds and to compare the drug-likeness of the isomer compounds with standard drugs.

For both isomer compounds, the miLogP values are less than five, number of H-bond acceptor was two, molecular weight of the isomer compounds were less than 500 g per mole, and number of H-bond donor was detected to be one. The isomer compounds have zero rotatable bond and topological polar surface area (TPSA) is 32.86 $Å^2$. Due to the absence of rotatable bonds and lowest TPSA value, the present isomer compounds can be passed in aqueous blood and penetrate the lipid-based cell membrane to reach the core of a cell [68].

Thus, the physiochemical properties (Table 7) obtained for isomer compounds satisfy Lipinski's rule of five, which preliminarily suggests the drug-likeness of the isomer compounds. Hence, the drug-likeness of our isomer compounds is comparable with standard drug.

The 4CMQ isomer compounds of ADMET and toxicity parameters were computed using pre-ADMET online server and the values are gathered in Tables 8 and 9, respectively. The human intestinal absorption (HIA) percentage for isomer compounds and standard drugs are above 95% which predicts these are potent drug agent. The isomer compounds are strongly interacting with plasma protein when compared with ciprofloxacin and fluconazole as evidenced from the plasma protein binding percentage (88.28% for 4C6MQ and 70.73% for 4C8MQ). The absorption parameter Caco-2 cell permeability of the isomer compounds is 24.43 nm/s and MDCK cell permeability scores are 67.18 and 55.07 nm/s for 4C6MQ

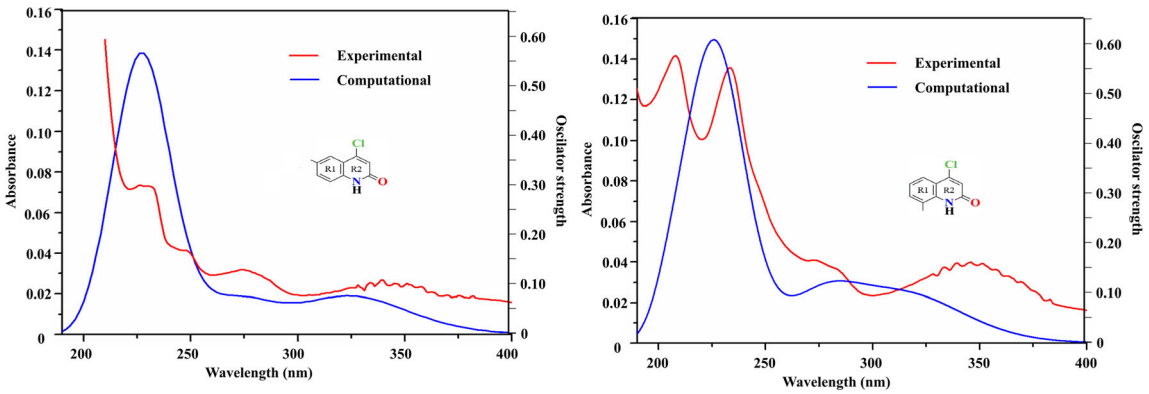

Fig. 9 UV Spectrum for 4CMQ isomer by experimental and TD-DFT approach

Table 7 Molinspiration property values of 4CMQ isomer, ciprofloxacin, and fluconazole

Compound	mi LogP[a]	Topological polar surface area	Molecular weight	No. of H-bond acceptors	No. of H-bond donors	No. of violations	Volume	*n* atoms	Number of rotatable bonds
4C6MQ	2.49	32.86	193.63	2	1	0	162.10	13	0
4C8MQ	2.47	32.86	193.63	2	1	0	162.10	13	0
Ciprofloxacin	− 0.70	74.57	331.35	6	2	0	285.46	24	3
Fluconazole	− 0.12	81.66	306.28	7	1	0	248.96	22	5

[a] Logarithm of partition coefficient between n-octanol and water (miLogP)

Table 8 ADMET property values of 4CMQ isomer with ciprofloxacin and fluconazole using pre-ADMET online server

Compound	Absorption				Distribution	
	Human intestinal absorption (HIA %)	CaCo-2 cell permeability (nm/s)	MDCK cell permeability (nm/s)	Skin permeability (logkp, cm/h)	Plasma protein binding (%)	Blood-brain barrier penetration (c.brain/c.blood)
4C6MQ	97.25	24.43	67.18	− 2.60	88.28	0.8379
4C8MQ	97.25	24.43	55.07	− 2.65	70.73	0.8378
Ciprofloxacin	96.27	21.28	10.30	− 4.60	31.05	0.0136
Fluconazole	95.59	17.23	1.84	− 4.18	55.16	0.2470

and 4C8MQ isomer compounds, respectively, which are higher than the standard drug. The blood-brain barrier (BBB) penetration parameter is associated with central nerves system (CNS) affecting behavior of the compound [69]. The BBB values of the isomer compounds and standard drug predict inactive against CNS. Both the isomer compounds have positive and negative carcinogen prediction in mouse and rat, respectively, as shown in Table 9. The carcinogen predictions of isomer compounds are comparable to standard drug.

The isomer compounds are predicted of being possessed with remarkable biological activity, from their pharmacological properties. Moreover this also is a capable inhibitor for microbial diseases among the standard drug.

Molecular docking analysis

The pharmacological results motivate to analyze the docking interaction of isomer compounds with target protein like DNA gyrase enzyme for bacterial and lanosterol 14 α-demethylase enzyme for fungal.

4CMQ-3G75 complex

To investigate the anti-bacterial activity of the isomer compounds, they were docked with anti-bacterial target protein DNA gyrase enzyme (PDB ID: 3G75). The molecular docking binding energy, bonding type and bond separation was obtained and presented in Table 10. The interactions obtained in isomer compounds and ciprofloxacin with target protein 3G75 were displayed in Fig. 10. In 4C6MQ-3G75 and 4C8MQ-3G75 complexes, the ligands were interacted with amino acid residues GLY85, ASP81, ARG84, and PRO87.

In 3G75-4C6MQ complex, the oxygen (O1) atom of 4C6MQ has branched H-bond polar interaction with the atom N2 and N3 of residue GLY85 and ARG84 at a distance of 2.139 and 3.069 Å, respectively. Moreover, the nitrogen atom of 4C6MQ interacts with atom OD1 of ASP81 at a separation of 2.140 Å. Likewise, π-alkyl hydrophobic interaction can be noticed between five-membered ring of PRO87 and the chlorine atom Cl1 of 4C6MQ (distance = 4.690 Å).

Table 9 Toxic parameters of 4CMQ isomer, ciprofloxacin, and fluconazole using pre-ADMET online server

Compound	Carcinogenicity(Mouse)	Carcinogenicity(Rat)
4C6MQ	Carcinogen	Non-carcinogen
4C8MQ	Carcinogen	Non-carcinogen
Ciprofloxacin	Non-carcinogen	Non-carcinogen
Fluconazole	Non-carcinogen	Carcinogen

Table 10 Binding energy, hydrogen bond, and hydrophobic contacts of 4CMQ isomer compounds and Ciprofloxacin with 3G75

Inhibitor	Binding energy kcal m^{-1}	Interactions	Distance Å	Bonding	Bonding types	Binding site of protein	Binding site of ligand
4C6MQ	− 4.89	GLY85 [N2–H2 … O1]	2.139	Hydrogen	H-bond	N2	O1
		[N1–H1 ... OD1] ASP81	2.140	Hydrogen	H-bond	OD1	N1
		ARG84 [N3–H3 … O1]	3.069	Hydrogen	H-bond	N3	O1
		PRO87 [CD … Cl1]	3.695	Hydrogen	CH-bond	CD	Cl1
		PRO87 [π … Cl1]	4.690	Hydrophobic	π-Alkyl	5-membered ring	Cl1
4C8MQ	− 4.83	GLY85 [N2–H2 … O1]	2.017	Hydrogen	H-bond	N2	O1
		[N1–H1 ... OD1] ASP81	2.044	Hydrogen	H-bond	OD1	N1
		ARG84 [H3–N3 … O1]	3.039	Hydrogen	H-bond	N3	O1
		PRO87 [π … Cl1]	4.865	Hydrophobic	π-Alkyl	5-membered ring	Cl1
Ciprofloxacin	− 4.01	ARG144 [N1–H1 … O21]	3.845	Hydrogen	H-bond	N1	O21
		GLY85 [O21–H13 ... O]	3.431	Hydrogen	H-bong	O21	O
		PRO87 [CD … π]	3.925	Hydrophobic	Sigma-π	CD	Pyridine ring

Similarly, other complex 3G75-4C8MQ also induce the same type of interaction with 3G75 (Table 10). Both complexes exhibit more interactions when compared to ciprofloxacin-3G75 complex. Further, the binding energy of isomer 4C6MQ and 4C8MQ complexes are − 4.79 and − 4.83 kcal/mol, respectively, which is higher than ciprofloxacin complex binding energy (− 4.01 kcal/mol). The results of docking showed that isomer compounds exert DNA gyrase enzyme inhibitory activity and thereby act as a good medicine for bacterial diseases.

4CMQ-1EA1 complex

To investigate the antifungal activity of the isomer compounds, they were docked with antifungal target lanosterol 14 α-demethylase enzyme (PDB ID:1EA1). The molecular docking binding energy, bonding type, and bond separation was acquired and listed in Table 11. The ligand interactions of 4CMQ-1EA1 complexes were shown in Fig. 11.

In 4C6MQ-1EA1 complex, the residue ILE323 has bifurcated H-bond interaction with N1 and O1 atom of isomer compound 4C6MQ at a distance 3.077 and 3.011 Å, respectively. The benzene ring of 4C6MQ has splitting hydrophobic sigma-π and π … π interactions with CD2 atom of LEU321 and six-membered ring of PHE78 at a distance of 3.639 and 5.397 Å, respectively. The six-membered ring of PHE78 and five-membered ring of HIS259 has π … π and π-alkyl hydrophobic interactions with pyridine ring and chlorine atom of 4C6MQ at a separation 5.612 and 3.905 Å, respectively.

In 4C8MQ-1EA1 complex, the O1 atom of 4C8MQ has connected with NE2 atom of HIS259 and N atom of VAL435 by H-bond at a distance 2.935 and 2.860 Å, respectively. Likewise, the nitrogen atom of ILE323 residue interacts with Cl1 atom of 4C8MQ via H-bond forming a distance of 3.295 Å. A π–π hydrophobic interaction between the six-membered ring of PHE78 and benzene ring of 4C8MQ also observed at a distance 4.932 Å. Moreover, the binding energy of 4C6MQ-1EA1, 4C8MQ-1EA1, and fluconazole-1EA1 complexes are − 4.32, − 4.39, and − 3.59 kcal/mol, respectively.

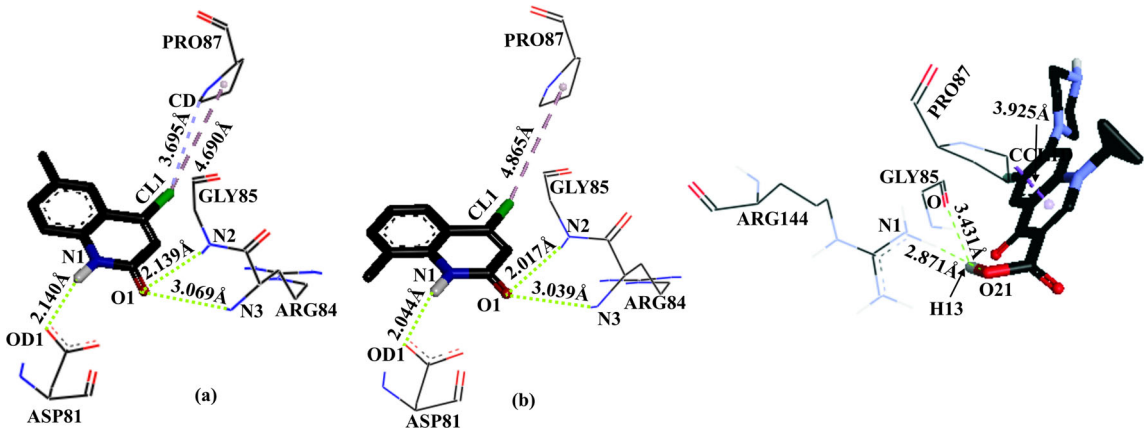

Fig. 10 Interaction of **a** 4C6MQ, **b** 4C8MQ, and **c** ciprofloxacin to 3G75 binding site

Table 11 Binding energy, hydrogen bond, and hydrophobic contacts of 4CMQ isomer and fluconazole with 1EA1

Inhibitor	Binding energy kcal m^{-1}	Interactions	Distance Å	Bonding	Bonding types	Binding site of protein	Binding site of ligand
4C6MQ	− 4.39	ILE323 [N–H … O1]	3.077	Hydrogen	H-bond	N	O1
		[N1–H1 … O] ILE323	3.011	Hydrogen	H-bond	O	N1
		LEU321 [CD2 … π]	3.639	Hydrophobic	Sigma-π	CD2	C1–C6 Benzene ring
		PHE78 [π … π]	5.397	Hydrophobic	π … π	6-membered ring	C1–C6 Benzene ring
		PHE78 [π … π]	5.612	Hydrophobic	π … π	6-membered ring	Pyridine ring
		HIS259 [π … Alkyl]	3.905	Hydrophobic	π–alkyl	5-membered ring	Cl1
4C8MQ	− 4.32	HIS259 [NE2–HE2 … O1]	2.935	Hydrogen	H-bond	NE2	O1
		VAL435 [N–H … O1]	2.860	Hydrogen	H-bond	N	O1
		ILE323 [N–H … Cl1]	3.295	Hydrogen	H-bond	N	Cl1
		PHE78 [π … π]	4.932	Hydrophobic	π … π	6-membered ring	C1–C6 Benzene ring
Fluconazole	− 3.59	ARG96 [N1–H1 … N18]	3.489	Hydrogen	H-bond	N1	N18
		ARG96 [N1–H2 … N18]	3.354	Hydrogen	H-bond	N1	N18
		HIS259 [NE2–HE2 … F2]	3.343	Hydrogen	H-bond	NE2	F2
		ILE323 [N–H … F1]	3.860	Hydrogen	H-bond	N	F1
		LEU321 [π … CG]	3.693	Hydrophobic	π-Sigma	Difluorobenzene	CG
		TYR76 [π–π]	4.160	Hydrophobic	π … π	6-membered ring	1,2,3-Triazole
		PHE78 [π–π]	5.247	Hydrophobic	π … π	6-membered ring	Difluro-4-nitro-benzene
		PHE225 [π–π]	4.556	Hydrophobic	π … π	6-membered ring	1,2,3-Triazole

The higher binding affinity which is based on the H-bond and hydrophobic interaction in isomer ligand-protein complexes discloses that isomer compounds exert Lanosterol 14 α-demethylase enzyme inhibitory activity and possibly will act as an anti-drug agent for fungal diseases.

Interpretation of antimicrobial activity

The pharmacological and docking results encouraged us to execute in vitro studies. The outcomes of the anti-bacterial and antifungal studies by Kirby Bauer disk diffusion methods are presented in Table 12. According to the result emulated through this research, the isomer compounds performed gradually raising scores of inhibition against the tested microorganisms. Thus, the 4CMQ isomer compounds reveals the antibacterial activity as moderate to good against *P. aeruginosa* and as mild to moderate against *E. coli* and *S. aureus* when compared with ciprofloxacin. Finally, moderate to good antifungal activity against *M. purpureus* and *P. citrinum* was revealed by both the isomer compounds and the least antifungal activity was revealed by the compound 4C6MQ towards *A. niger* when compared to the fluconazole. From the result, it is obvious that 4C6MQ has the highest antimicrobial activity compared to 4C8MQ compound. The comparative responses

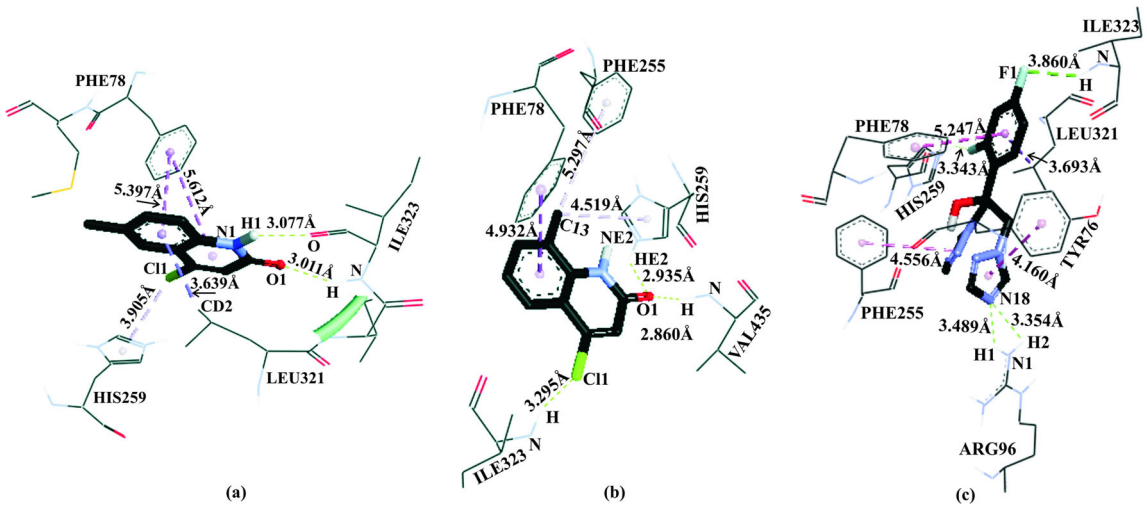

Fig. 11 Interaction of **a** 4C6MQ, **b** 4C8MQ, and **c** fluconazole to 1EA1 binding site

Table 12 Antimicrobial activity of 4CMQ isomer compound at different concentrations against bacterial and fungal pathogens

Microorganisms	4C6MQ			4C8MQ			Positive control 25 μg/ml
	Zone of inhibition (mm)			Zone of inhibition (mm)			
	Compound concentration			Compound concentration			
	25 μg/ml	50 μg/ml	75 μg/ml	25 μg/ml	50 μg/ml	75 μg/ml	
Bacterial pathogens	–	–	–	–	–	–	Ciprofloxacin
Staphylococcus aureus (MTCC 10623)	17	17	20	18	19	20	21
Escherichia coli (MTCC 443)	29	31	33	29	30	35	32
Pseudomonas aeruginosa (MTCC 1435)	30	34	40	31	32	38	35
Fungal pathogens	–	–	–	–	–	–	Fluconazole
Penicillium citrinum (NCIM768)	10	14	17	10	14	16	16
Aspergillus niger (MTCC281)	5	11	12	8	11	13	14
Monascus purpureus (MTCC369)	18	21	21	19	21	24	22

Values are mean of three independent experiments

of isomer compounds and standard drug against all microbial species are shown in Figs. 12 and 13.

The antimicrobial outcomes disclosed that isomer compounds exert pathogen inhibitory activity and possibly will act as potent anti-drug agent for bacterial and fungal diseases. Thus, the novel isomer 4-chloromethyl quinoline compounds disclose the effective antimicrobial properties which could be used as an effective antimicrobial agent, particularly for the treatment of multidrug resistant infections.

Conclusions

4-chloro-6-methylquinoline-2(1H)-one and its isomer 4-chloro-8-methylquinoline-2(1H)-one were synthesized. One of the isomer compound 4-chloro-6-methylquinoline-2(1H)-one was characterized and confirmed by SCXRD method. Both the isomer compounds have been characterized by FTIR, FT-Raman, UV-Vis, and NMR spectroscopy and compared with computational results, which have been exactly coincided. The NBO investigation substantiates the inter charge transmission in both isomer compounds and the possibility of bioactivity. The MEP polarity region and HOMO-LUMO energy values are confirmed the biological activity of the isomer compounds. The TD-DFT computational result has close agreement with UV-Vis spectrum data and which predicts the $n \rightarrow \pi^*$ transition between the molecular orbitals. Further, physiochemical and ADMET properties confirm the drug likeness and non-toxic behavior of isomer compounds. The good docking scores obtained for the isomer ligand-protein complexes reveals the inhibition nature of the isomer compounds against DNA gyrase and lanosterol 14 α-

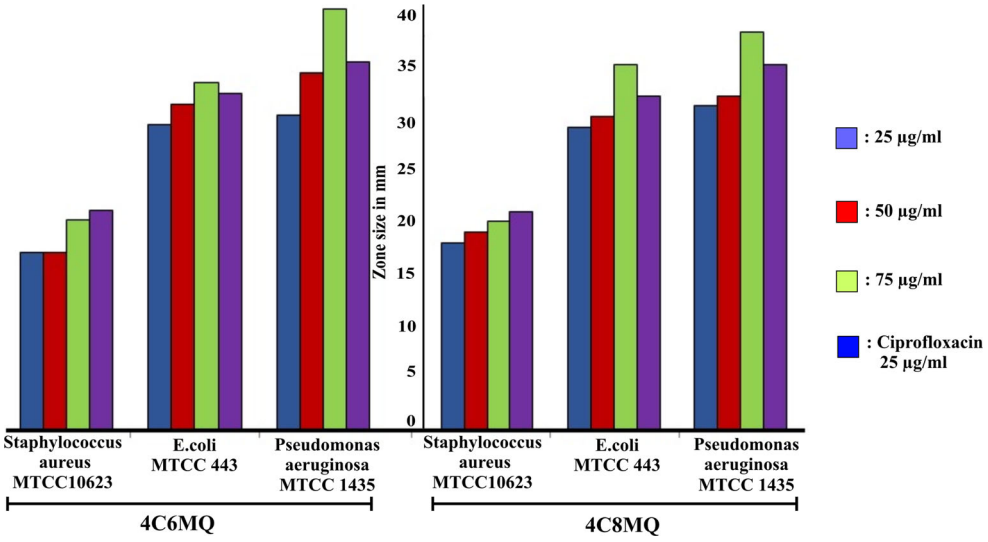

Fig. 12 A bar diagram for the antibacterial activity of 4CMQ isomer compounds

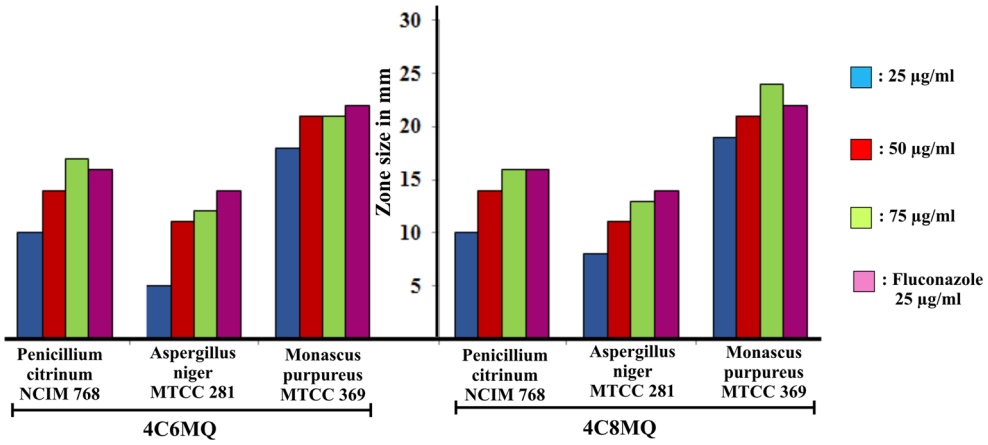

Fig. 13 A bar diagram for the antifungal activity of 4CMQ isomer compounds

demethylase enzymes. Further, the in vitro antimicrobial result confirms that the synthesized novel 4CMQ isomer compounds are very eye-catching antimicrobial drugs and can help as an excellent platform for the treatment of multidrug resistant infections. Hence, we hope that the isomer compounds may be after a systematic in vivo analysis and may be the best anti-drug agents for microbial diseases in future.

Acknowledgements The authors thank SAIF, IIT-Chennai, for the single-crystal XRD measurements and spectral studies.

Compliance with ethical standards

Conflict of interest The authors declare that they have no competing interests.

References

1. Michael JP (2008) Quinoline, quinazoline and acridone alkaloids. Nat Prod Rep. https://doi.org/10.1039/B612168N
2. Narender T, Shweta K, Tanvir KMS, Rao K, Srivastava SKP (2005) Prenylated chalcones isolated from Crotalaria genus inhibits in vitro growth of the human malaria parasite Plasmodium falciparum. Bioorg Med Chem Lett. https://doi.org/10.1016/j.bmcl.2005.03.081
3. Kidwai M, Bhushan KR, Sapra P (2000) Alumina-supported synthesis of antibacterial quinolines using microwaves. Bioorg Med Chem Lett. https://doi.org/10.1016/S0968-0896(99)00256-4
4. Nayyar A, Malde A, Coutinho E, Jain R (2006) Synthesis, antituberculosis activity, and 3D-QSAR study of ring-substituted-2/4-quinolinecarbaldehyde derivatives bioorg. Med Chem. https://doi.org/10.1016/j.bmc.2006.06.049
5. Hector RF (2005) An overview of antifungal drugs and their use for treatment of deep and superficial mycoses in animals. Clin Tech Small Anim Pract. https://doi.org/10.1053/j.ctsap.2005.07.005
6. Sharma V, Mehta DK, Das R (2017) Synthetic methods of quinoline derivatives as potent anticancer agents. Mini Rev Med Chem. https://doi.org/10.2174/1389557517666170510104954
7. Burnett JC, Opsenica D, Sriraghavan K, Panchal RK, Ruthel G, Ngyuen TL (2007). J Med Chem 50:2127–2136
8. Narender T, Shweta, Tanvir K, Rao MS, Srivastava K, Puri SK (2005). Bioorg Med Chem Lett 15:2453–2455
9. Cross RM, Monastyrskyi A, Mutka TS, Burrows JN, Kyle DE, Manetsch R (2010) Optimization: structure-activity and structure-property relationship studies of 3-substituted 2-methyl-4-(1H)-quinolones with antimalarial activity. J Med Chem 53:7076–7094
10. Kumar S, Bawa S, Gupta H (2009) Biological activities of quinoline derivatives. Mini-Rev Med Chem 9:1648–1654
11. Desai NC, Patel BY, Dave BP (2016) Synthesis and antimicrobial activity of novel quinoline derivatives bearing pyrazoline and pyridine analogues. Med Chem Res 26(1):109–119
12. Maity S, Khan SA, Ahmad S (2012) Synthesis, characterization, antimicrobial and antioxidant activity of some novel Schiff base derived from quinoline. Int J Pharm Biol Sci 2(3):90–98
13. Desai NC, Dodiya A, Shihory N (2013) Synthesis and antimicrobial activity of novel quinazolinone-thiazolidine-quinoline compounds. J Saudi Chem Soc 17(3):259–267
14. Vaidya A, Jain AK, Kumar P, Kashaw SK, Agrawal RK (2011) Predicting anti-cancer activity of quinoline derivatives: CoMFA and CoMSIA approach. J Enzyme Inhib Med Chem 26(6):854–861
15. Romano E, Castillo MV, Pergomet JL, Zinczuk J, Brandan SA (2012) Synthesis and structural and vibrational analysis of (5,7-dichloro-quinolin-8-yloxy) acetic acid. J Mol Struct. https://doi.org/10.1016/j.molstruc.2012.03.013
16. Lakshmi A, Balachandran V, Janaki A (2011) Comparative vibrational spectroscopic studies, HOMO-LUMO and NBO analysis of 5,7-dibromo-8-hydroxyquinoline and 5,7-dichloro-8-hydroxyquinoline based on density functional theory. J Mol Struct. https://doi.org/10.1016/j.molstruc.2011.07.022
17. Delgado JN, Remers WA (eds) (1998) Wilson and Gisvold's text book of organic medicinal and pharmaceutical chemistry10th edn. Lippincott-Raven, Philadelphia
18. Foroumadi A, Emami S, Mehni M, Moshafi MH, Shafiee A (2005). Bioorg Med Chem Lett 15:4536–4539
19. Bolakatti G, Katagi MS, Mamledesai SN, Sujatha ML, Dabadi P, Miskin N (2012) RGUHS. J Pharm Sci 2:60–66
20. Jayashree BS, Thomas S, Nayak Y (2010). Med Chem Res 19:193–209
21. Kraus JM, Tatipaka HB, McGuffin SA, Chennamaneni NK, Karimi M, Arif J, Verlinde CLMJ, Buckner FS, Gelb MH (2010). J Med Chem 53:3887–3898
22. Joseph B, Darro F, Be'hard A, Lesur B, Collignon F, Decaestecker C, Frydman A, Guillaumet G, Kiss R (2002). J Med Chem 45:2543–2555
23. Ismai MM, Abdel-Megid M, Hassan MM (2004) Some reactions of 2- and 4-substituted 8-methyl- quinolin-2(1H)-ones and their thio analogues. Chem Pap 58(2):117–125
24. Eakin AE, Green O, Hales N et al (2012) Pyrrolamide DNA gyrase inhibitors: fragment-based nuclear magnetic resonance screening to

identify antibacterial agents. Antimicrob Agents Chemother. https://doi.org/10.1128/AAC.05485-11
25. Rozman D (2000) Lanosterol 14α-demethylase (CYP51)—a cholesterol biosynthetic enzyme involved in production of meiosis activating sterols in oocytes and testis—a mini review. Pflugers Arch-Eur J Physiol. https://doi.org/10.1007/BF03376522
26. Ziegler E, Gelfert K (1959). Monatsh Chem 90:822–826
27. Bruker (2004) APEX-II, SAINT-plus (Version 7.06a). BrukerAXS Inc, Madion
28. Sheldrick GM (1996) SADABS. University of Gottingen, Gottingen
29. Sheldrick GM (2008) A short history of SHELX. Acta Crystallogr. https://doi.org/10.1107/S0108767307043930
30. Farrugia LJ (2012) WinGX and ORTEP for windows: an update. J Appl Crystallogr. https://doi.org/10.1107/S0021889812029111
31. Spek AL (2003) Single-crystal structure validation with the program PLATON. J Appl Crystallogr. https://doi.org/10.1107/S0021889802022112
32. Bruno IJ, Cole JC, Edgington PR, Kessler MK, Macrae CF, McCabe P, Pearson J, Taylor R (2002). Acta Cryst B. https://doi.org/10.1107/S0108768102003324
33. Biemer JJ (1973) Antimicrobial susceptibility testing by the Kirby-Bauer disc diffusion method. Ann Clin Lab Sci 2(3):135–140
34. Bauer AW, Kirby WMM, Sherris JC, Turck M (1966) Antibiotic susceptibility testing by a standardized single disk method. Am J Clin Pathol 45:493–496
35. Frisch MJ, Trucks G. W, Schlegel HB, Scuseria GE, Robb MA, Cheeseman JR, Montgomery JA, Vreven T, Kudin KN, Burant JC, Millam JM, Iyengar SS, Tomasi J, Barone V, Mennucci B, Cossi M, Scalmani G, Rega N, Petersson GA, Nakatsuji H, Hada M, Ehara M, Toyota K, Fukuda R, Hasegawa J, Ishida M, Nakajima T, Honda Y, Kitao O, Nakai H, Klene M, Li X, Knox JE, Hratchian HP, Cross JB, Bakken V, Adamo C, Jaramillo J, Gomperts R, Stratmann RE, Yazyev O, Austin AJ, Cammi R, Pomelli C, Ochterski JW, Ayala PY, Morokuma K, Voth GA, Salvador P, Dannenberg JJ, Zakrzewski VG, Dapprich S, Daniels AD, Strain MC, Farkas O, Malick DK, Rabuck AD, Raghavachari K, Foresman JB, Ortiz JV, Cui Q, Baboul AG, Clifford S, Cioslowski J, Stefanov BB, Liu G, Liashenko A, Piskorz P, Komaromi I, Martin RL, Fox DJ, Keith T, Al-Laham MA, Peng CY, Nanayakkara A, Challacombe M, Gill PMW, Johnson B, Chen W, Wong MW, Gonzalez C, Pople JA (2004) Gaussian Inc., Wallingford
36. Becke AD (1993) Density-functional thermochemistry. III The role of exact exchange. J Chem Phys. https://doi.org/10.1063/1.464913
37. Becke AD (1988) Density-functional exchange-energy approximation with correct asymptotic behavior. Phys Rev A. https://doi.org/10.1103/PhysRevA.38.3098
38. Sundaraganesan N, Ilakiamani S, Saleem H, Wojciechowski PM, Michalska D (2005) FT-Raman and FT-IR spectra, vibrational assignments and density functional studies of 5-bromo-2-nitropyridine. Spectrochim Acta A. https://doi.org/10.1016/j.saa.2004.11.016
39. Karabacak M, Kurt M, Cınar M, Coruh A (2009) Experimental (UV, NMR, IR and Raman) and theoretical spectroscopic properties of 2-chloro-6-methylaniline. Mol Phys. https://doi.org/10.1080/00268970902821579
40. Foresman JB, Frisch Æ (1996) Exploring chemistry with electronic structure methods, 2nd edn. Gaussian Inc., Pittsburgh
41. Molinspiration Cheminformatics, Bratislava, Slovak Republic. Available at: http://www.molinspiration.com/services/properties.html accessed 16 February 2018
42. Lipinski CA, Lombardo F, Dominy BW, Feeney PJ (1997) Experimental and computational approaches to estimate solubility and permeability in drug discovery and development settings. Adv Drug Deliv Rev. https://doi.org/10.1016/S0169-409X(96)00423-1
43. Murugavel S, Sundramoorthy S, Lakshmanan D, Subashini R, Pavan Kumar P (2017) Synthesis, crystal structure analysis, spectral (NMR, FT-IR, FT-Raman and UV–Vis) investigations, molecular docking studies, antimicrobial studies and quantum chemical calculations of a novel 4-chloro-8-methoxyquinoline-2(1H)-one: an effective antimicrobial agent and an inhibition of DNA gyrase and lanosterol-14α-demethylase enzymes. J Mol Struct. https://doi.org/10.1016/j.molstruc.2016.11.035
44. Available at: www.preadmet.com accessed 16 February 2018
45. Morris GM, Huey R, Lindstrom W, Sanner MF, Belew RK, Goodsell DS, Olson AJ (2009) Autodock4 and AutoDockTools4: automated docking with selective receptor flexiblity. J Comput Chem. https://doi.org/10.1002/jcc.21256
46. Morris GM, Goodsell DS, Halliday RS, Huey R, Hart WE, Belew RK, Olson AJ (1998) Automated docking using a Lamarckian genetic algorithm and an empirical binding free energy function. J Comput Chem. https://doi.org/10.1002/(SICI)1096-987X(19981115)19:14<1639::AID-JCC10>3.0.CO;2-B
47. Discovery studio visualizer: http://accelrys.com/products/collaborative-science/biovia-discovery-studio/visualization.html
48. Murugavel S, Ranjith S, SubbiahPandi A, Periyasami G, Raghunathan R (2009) Crystal structure of (E)-N-(3,3-diphenylallylidene)-9-ethyl-9H-carbazol-3-amine. Acta Cryst E. https://doi.org/10.1107/S2056989015005770
49. Binil PS, Mary YS, Varghese HT, Paniker CY, Anoop MR, Manojkumar TK (2012) Infrared and Raman spectroscopic analyses and theoretical computation of 4-butyl-1-(4-hydroxyphenyl)-2-phenyl-3,5-pyrazolidinedione. Spectrochim Acta A. https://doi.org/10.1016/j.saa.2012.03.014
50. Sert Y, Cirak C, Ucun F (2013) Vibrational analysis of 4-chloro-3-nitrobenzonitrile by quantum chemical calculations. Spectrochim Acta A. https://doi.org/10.1016/j.saa.2013.01.046
51. John NL, Joy LK, Saravana Kumar M, Shaiju SS, Subashini A, Sajan D (2017) Quantitative structure and activity relationship on the biological, nonlinear and the spectroscopic properties of the Schiff base material: 4-chloro-4'bromobenzylidene aniline. Mol Simul. https://doi.org/10.1080/08927022.2017.1337272
52. Ghalla H, Issaoui N, Govindarajan M, Flakus HT, Jamroz MH, Oujia B (2014) Spectroscopic and molecular structure investigation of 2-furanacrylic acid monomer and dimer using HF and DFT methods. J Mol Struct 1059:132–143
53. Mohan J (2011) Organic spectroscopy-principles and applicationssecond edn. Narosa Publishing House, New Delhi, p 30
54. Bellamy J (1975) Advances in Infra-red group frequencies, vol 2. Third edn. Chapman and Hall, London
55. Varsanyi G (1969) Vibrational spectra of benzene derivatives. Academic press, New York
56. Dollish FR, Fateley WG, Bentley FF (1997) Characteristic Raman frequencies of organic compounds. John Wiley & Sons, New York
57. Tonannavar J, Yenagi J (2012) Vibrational spectra, normal modes, ab initio and DFT calculations for 6-chloro- and 7-chloro-4-bromomethylcoumarins. Spectrochim Acta A. https://doi.org/10.1016/j.saa.2010.03.013
58. Obafemi CA, Fadare OA, Jasinski JP, Millikan SP, Obuotor EM, Iwalewa EO, Famuyiwa SO, Sanusi K, Yilmaz Y, Ceylan Ü (2017) Microwave-assisted synthesis, structural characterization, DFT studies, antibacterial and antioxidant activity of 2-methyl-4-oxo-1,2,3,4-tetrahydroquinazoline-2-carboxylic acid. J Mol Struct. https://doi.org/10.1016/j.molstruc.2017.11.018
59. Silverstein RM, Bassler GC, Morrill TC (1974) Spectrometric identification of organic compounds3rd edn. John Wiley & Sons, New York, p 239
60. Socrates G (2011) Infrared and Raman characteristic group frequencies: tables and charts. Wiley, New York

61. Murugavel S, Vetri Velan V, Kannan D, Bakthadoss M (2016) Experimental and computational approaches of a novel methyl (2E)-2-{[N-(2-formylphenyl)(4-methylbenzene)sulfonamido]methyl}-3-(4-chlorophenyl)prop-2-enoate: a potential antimicrobial agent and an inhibition of penicillin-binding protein. J Mol Struct. https://doi.org/10.1016/j.molstruc.2016.02.084
62. Katritzky AR, Ellison J, Frank J, Raikoczy P, Radics L, Gacs-Baitz E (1981) ^{13}C NMR spectra of 4-quinolones and related compounds. Org Magn Reson 16(4):280–284
63. Bagno A, Rastrelli F, Saielli G (2003) Predicting 13C NMR spectra by DFT calculations. J Phys Chem A. https://doi.org/10.1021/jp0353284
64. Murugavel S, Jacob Prasanna Stephen CS, Subashini R, Raveendranatha Reddy H, AnanthaKrishnan D (2016) Synthesis, crystal structure investigation, spectroscopic characterizations and DFT computations on a novel 1-(2-chloro-4-phenylquinolin-3-yl)ethanone. J Mol Struct. https://doi.org/10.1016/j.molstruc.2016.05.095
65. Kuruvilla TK, Prasana JC, Muthu S, George J, Mathew SA (2018) Quantum mechanical and spectroscopic (FT-IR, FT-Raman) study, NBO analysis, HOMO-LUMO, first order hyperpolarizability and molecular docking study of methyl[(3R)-3-(2-methylphenoxy)-3-phenylpropyl]amine by density functional method. Spectrochim Acta A. https://doi.org/10.1016/j.saa.2017.07.029
66. Bougharraf H, Benallal R, El Faydy M, Mondieig D, Negrier P, Sahdane T, Kabouchi B, Lakhrissi B, Zawadzka A (2016) Synthesis, spectroscopic characterization, x-ray analysis, and DFT-HF calculations of 5-ethoxymethyl8-hydroxyquinoline. Opt Quant Electron. https://doi.org/10.1007/s11082-016-0393-5
67. Diwaker (2014) Quantum mechanical and spectroscopic (FT-IR, 13C, 1H NMR and UV) investigations of 2-(5-(4-Chlorophenyl)-3-(pyridin-2-yl)-4,5-dihydropyrazol-1-yl)benzo[d]thiazole by DFT method. Spectrochim Acta A. https://doi.org/10.1016/j.saa.2014.02.196
68. Khoshneviszadeh M, Shahraki O, Khoshneviszadeh M, Foroumadi A, Firuzi O (2016) Structure-based design, synthesis, molecular docking study and biological evaluation of 1,2,4-triazine derivatives acting as COX/15-LOX inhibitors with anti-oxidant activities. J Enzyme Inhib Med Chem. https://doi.org/10.3109/14756366.2016.1158713
69. Banks WA (2009) Characteristics of compounds that cross the blood-brain barrier. BMC Neurol. https://doi.org/10.1186/1471-2377-9-S1-S3